Ferroelectric phase transition of the disubstituted diacetylene 1,6-bis(2,4-dinitrophenoxy)-2,4-hexadiyne: Analysis by NMR and x-ray studies

Hubert Winter* and Elmar Dormann*
Physikalisches Institut and Bayreuther Institut für Makromolekülforschung (BIMF), Universität Bayreuth, Postfach 101251, W-8580 Bayreuth, Germany

M. Bertault and L. Toupet
Groupe de Physique Cristalline, Université de Rennes 1, Campus de Beaulieu, F-35042 Rennes CEDEX, France
(Received 8 April 1992)

Proton-NMR and x-ray measurements were used to analyze the ferroelectric phase transition of the disubstituted diacetylene 1,6-bis(2,4-dinitrophenoxy)-2,4-hexadiyne (DNP), in which the phase transition is accompanied by a molecular twisting. Proton-spin-latttice relaxation is analyzed as function of Larmor frequency, temperature, and orientation of the single crystals. The molecular motions relevant for the dielectric phase transition and causing the loss of the center of symmetry of DNP single crystals are reflected by these NMR results and by detailed x-ray analysis at three different temperatures.

I. INTRODUCTION

Single crystals of the disubstituted diacetylene DNP [1,6-bis(2,4-dinitrophenoxy)-2,4-hexadiyne] show very interesting dielectric properties:[1,2] if the temperature is lowered from room temperature, the b-axis low-frequency electric permittivity increases for temperatures below 120 K and reaches maximum values of about 100 at a transition temperature of about $T_c=(46\pm1)$ K. Below the transition temperature, spontaneous electric polarization is observed in the crystallographic b direction reaching values of about 1.6×10^{-3} cm^{-2} at 10 K, while the permittivity decreases again with decreasing temperature.[1] The room-temperature crystal structure of DNP is centrosymmetric, space group $P2_1/n$.[3,4] Two DNP molecules (Fig. 1) related by symmetry are accommodated in the monoclinic unit cell. The electric dipole moments of about 1×10^{-29} cm of the dinitrophenoxy substituent groups R in the disubstituted diacetylene molecule $R-C\equiv C-C\equiv C-R$ are compensated antiferroelectrically due to the individual DNP molecules' center of symmetry. The ferroelectric properties of the low-temperature phase indicate an intramolecular distortion, leading to an uncompensation of the side groups' electric dipole moments. The loss of the space group's mirror plane and an appropriate intramolecular distortion has been estimated from the dielectric properties.[1] Recently, it was shown that the low-temperature phase of DNP is ferroelectric.[5]

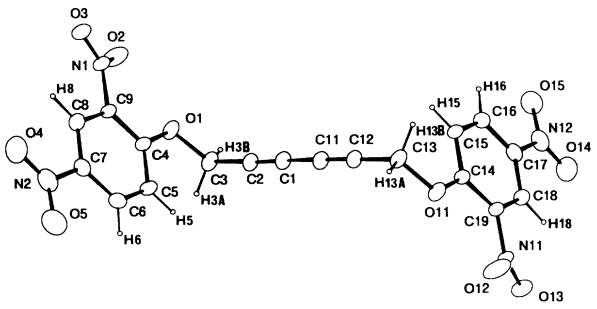

FIG. 1. Projection on (bc) plane along the a axis of the DNP molecule in the low-temperature phase and labeling of the atoms. In the high-temperature phase the labeling is the same for the two moieties of the molecule. The thermal ellipsoids are at 80% probability, except for the hydrogen atoms.

One of the peculiarities of DNP crystals is that its polymerization is only thermally initiated (and not by x rays), typically at 130°C (Refs. 2 and 6) and completely achieved after 16 or 17 h of annealing at that temperature. The polymer chain direction coincides with the crystallographic a axis and is perpendicular to the polar b axis. DNP polymer crystals of high perfection with up to about 95% polymer content can be obtained.

A second exothermic peak was also observed by differential scanning calorimetry upon a longer annealing time and was associated with an order-disorder transition in the polymer crystal.[3,6] Only the crystallographic order perpendicular to the polymer chain direction a is destroyed, however.[3]

The size of the anomaly of the electric permittivity, the transition temperature, and the amount of spontaneous polarization detected in the low-temperature range are greatly reduced for polymer contents of less than 15% already and suppressed below the sensitivity level of the dielectric measurements for fully polymerized samples. There is presently no simple explanation or clear understanding for this strong dependence on solid-state polymerization (SSP). Many details of the ferroelectric phase transition of DNP are not yet understood.

Therefore we used NMR in order to answer at least two of the most interesting questions: Why is the phase transition of DNP suppressed by the solid-state polymerization? and Can molecular motions be identified in the high-temperature phase of DNP that induce the phase

transition to the noncentrosymmetric low-temperature phase? Furthermore it appeared interesting to study the structure of the low-temperature phase to know whether DNP monomer crystals have a homogeneous low-temperature phase with weak uniform molecular distortion in every unit cell or if the above results stem from a nonuniform phase.

Our report is organized as follows. After a short mention of relevant experimental details in Sec. II, x-ray results will be reported in Sec. III and the results of proton NMR for DNP monomer crystals in Sec. IV. The orientation dependence of the NMR spectrum is analyzed in Sec. IV A and is used to detect a molecular reorientation at the phase transition in Sec. IV B. The analysis of the proton spin-lattice relaxation, measured as function of temperature, Larmor-frequency, and crystal orientation, is reported in Sec. IV C and reveals two types of molecular motions in DNP. We had to control the concentration of paramagnetic defects created during SSP in order to derive reproducible and reliable data on the temperature dependence of proton spin-lattice relaxation for partially polymerized DNP single crystals in Sec. IV D. The conclusions drawn from the NMR and x-ray analysis on the ferroelectric phase transition of DNP are summarized in Sec. V.

II. EXPERIMENTAL DETAILS

A. Crystal growth and polymerization

1,6-bis(2,4-dinitrophenoxy)-2,4-hexadiyne was prepared as described in detail before[1] and similar to the method introduced earlier by Kalyanaraman *et al.*[7] For crystal growth, DNP was dissolved in boiling acetone. The solvent was evaporated from the solution kept at 50 °C by a slow stream of nitrogen within one week, typically. For the NMR measurements, single crystals of about 10 mm in length and approximately quadratic cross section (e.g., 3×4 mm^2) were used. The a axis (or polymer chain direction) is parallel to the long crystal axis.

Partially or fully polymerized DNP crystals were obtained by thermal polymerization at 130 °C for different periods of time. Their polymer content was determined gravimetrically after completion of the NMR and magnetic susceptibility measurements. After grinding the respective crystal to powder, the DNP monomer was dissolved in boiling acetone and the weights of both the insoluble polymer and the soluble monomer portion were determined.

B. X-ray measurements

For the crystal structure measurements of DNP monomer small single crystals having the shape of a prism $(0.2\times0.2\times0.15)$ mm^3 in size and slightly red brown in color were used. The samples were studied in Rennes at three temperatures ($T=296$, 145, and 5 K)[4] on an automatic diffractometer CAD4 Enraf-Nonius with graphite monochromatized Mo $K\alpha$ radiation ($\lambda=0.71069$ Å).

The structures at 296 and 145 K were performed, respectively, directly at room atmosphere, and flushed with a stream of cold nitrogen gas. The structure at 5 K was performed on the diffractometer equipped with an helium gas flow cryostat FR 537 (Enraf-Nonius). All the calculations were performed on a Digital PDP 11/60 computer with the SDP package.[8] Atomic scattering factors come from International Tables for x-ray crystallography.[9]

C. Magnetic susceptibility measurements

The magnetic susceptibility of the polymerized and nonpolymerized samples were measured with a SQUID magnetometer (Quantum Design, San Diego: Magnetic Property Measurement System) for magnetic field strengths of up to 5.5 T in the temperature range 1.7–300 K. During the measurement the crystals were surrounded by a low-pressure helium atmosphere.

D. NMR measurements

The NMR measurements at 200, 60, and 31 MHz were performed on a Bruker CXP spectrometer with home-built probe heads. Fixed external fields of 4.7 T were applied with a superconducting magnet for 200 MHz NMR and variable fields up to 1.4 T for lower frequencies with an electromagnet. The resolution of the shown Fourier transform spectra is limited to 1.2 kHz due to the word length of our ADC.

The variable temperature results (4–300 K) were obtained using an Oxford Instruments CF 200 continuous flow cryostat and an home-built temperature controller. The longitudinal or spin-lattice relaxation time T_1 was determined from the saturation recovery using a pulse sequence with a saturation comb. The pulse spacing within the comb was set to 10 μs, the comb length was 20 pulses, and the pulse length amounted to 2.5 μs at 200 MHz or 2 μs at lower frequencies. Varying the time τ between the comb and the monitoring 90°-pulse between at most 10 min and at least 10 s gives the relaxation time T_1, which has been calculated from the area of the NMR spectra obtained by Fourier transformation of the FID. T_1 was derived for the full proton spectrum and the central line or the satellites (see Fig. 4, later) individually. No differences were observed outside the typical T_1 data fluctuations. Thus, only T_1 data characteristic for all protons of DNP (full spectrum) will be reported below.

III. X-RAY RESULTS FOR DNP MONOMER CRYSTALS

A. Monomer crystal data

The unit cell parameters were determined from the angles of 25 strong reflections. The structures were solved by direct methods using the program MULTAN 82.[10] After isotropic, then anisotropic refinements, the hydrogen atoms were located with a Fourier difference, then refined, except for the noncentrosymmetric structure at $T=5$ K. In this case, the anisotropic refinements lead to temperature factors not positive-definite for some atoms, on account of the correlations due to the pseudocentrosymmetricity of the pattern; it was possible to reduce

TABLE I. Positional parameters for DNP atoms and equivalent isotropic displacement parameters at $T=296$ K, with estimated standard deviation in parentheses.

Atom	X	Y	Z	B(Å^2)
*O*1	0.9315(3)	0.2173(2)	0.6693(1)	4.07(4)
*O*2	1.0270(4)	0.2446(2)	0.8442(1)	7.23(6)
*O*3	0.6992(4)	0.2908(2)	0.9076(1)	5.34(5)
*O*4	0.0817(4)	0.5526(2)	0.7611(2)	7.25(6)
*O*5	0.0119(5)	0.5601(2)	0.6131(2)	8.42(7)
*N*1	0.8088(4)	0.2834(2)	0.8411(1)	3.96(5)
*N*2	0.1288(5)	0.5258(2)	0.6857(2)	5.66(6)
*C*1	0.6018(5)	0.0352(2)	0.5166(2)	3.83(5)
*C*2	0.7747(5)	0.0964(2)	0.5443(2)	4.01(6)
*C*3	0.9788(5)	0.1743(3)	0.5822(2)	4.50(6)
*C*4	0.7363(5)	0.2918(2)	0.6692(2)	3.43(5)
*C*5	0.5904(5)	0.3355(2)	0.5897(2)	4.19(6)
*C*6	0.3962(5)	0.4122(2)	0.5954(2)	4.50(6)
*C*7	0.3432(5)	0.4451(2)	0.6798(2)	4.14.(6)
*C*8	0.4767(5)	0.4028(2)	0.7597(2)	3.75(5)
*C*9	0.6737(4)	0.3267(2)	0.7536(2)	3.28(5)
*H*3*A*	0.993(4)	0.238(2)	0.540(1)	4*
*H*3*B*	1.136(4)	0.137(2)	0.593(2)	4*
*H*5	0.625(4)	0.314(2)	0.530(2)	4*
*H*6	0.316(4)	0.445(2)	0.541(2)	4*
*H*8	0.440(4)	0.422(2)	0.822(2)	4*

these correlations with alternative refinements of each half molecule. The best full-matrix refinements gave the following results, with 161 variables (x,y,z,β_{ij} for C, O, and N atoms; x,y,z for H atoms) when the H atoms were refined, at $T=296$ K and $T=145$ K (B_{eq} fixed at 4 Å^2), and with 185 variables (x,y,z,β_{ij} for C, O, and N atoms; x,y,z for H atoms) when the H atoms were refined, at $T=5$ K (B_{eq} fixed at 2 Å^2): at $T=296$ K, as it was determined previously,[3] and at $T=145$ K, the crystal structure is centrosymmetric and monoclinic (space group $P2_1/n, Z=2$). At $T=296$ K [1742 reflections, 1219 independent with $I\geq 2\sigma(I)$], the final values are $R=0.040$, $R_\omega=0.038$, and $S_\omega=0.9$ ($R_{int}=0.017$). At $T=145$ K [1692 reflections, 1346 independent with $I\geq\sigma(I)$], the final values are $R=0.033$, $R_\omega=0.034$, and $S_\omega=0.9$ ($R_{int}=0.018$): at $T=5$ K the crystal structure is noncen-

TABLE II. Positional parameters for DNP atoms and equivalent isotropic displacement parameters at $T=145$, with estimated standard deviation in parentheses.

Atom	X	Y	Z	B(Å^2)
*O*1	0.9379(2)	0.2201(1)	0.66989(8)	2.16(3)
*O*2	1.0373(3)	0.2464(2)	0.8457(1)	3.62(3)
*O*3	0.7031(3)	0.2940(1)	0.90973(9)	2.70(3)
*O*4	0.0770(3)	0.5575(1)	0.7626(1)	3.91(4)
*O*5	0.0026(3)	0.5655(2)	0.6138(1)	4.57(4)
*N*1	0.8155(3)	0.2863(1)	0.8427(1)	2.05(3)
*N*2	0.1249(3)	0.5305(2)	0.6868(1)	3.08(4)
*C*1	0.6025(4)	0.0359(2)	0.5163(1)	2.05(4)
*C*2	0.7788(4)	0.0987(2)	0.5438(1)	2.15(4)
*C*3	0.9856(4)	0.1778(2)	0.5820(1)	2.45(4)
*C*4	0.7399(4)	0.2951(2)	0.6702(1)	1.85(3)
*C*5	0.5907(4)	0.3390(2)	0.5903(1)	2.31(4)
*C*6	0.3933(4)	0.4169(2)	0.5959(1)	2.48(4)
*C*7	0.3409(4)	0.4501(2)	0.6810(1)	2.25(4)
*C*8	0.4775(4)	0.4072(2)	0.7612(1)	2.06(4)
*C*9	0.6774(3)	0.3303(2)	0.7552(1)	1.74(3)
*H*3*A*	1.001(5)	0.243(2)	0.539(2)	4*
*H*3*B*	1.147(5)	0.139(2)	0.593(2)	4*
*H*5	0.625(4)	0.320(2)	0.531(2)	4*
*H*6	0.304(4)	0.451(2)	0.541(2)	4*
*H*8	0.440(4)	0.429(2)	0.821(2)	4*

trosymmetric and monoclinic (space group $P2_1$, $Z=2$) and for 1486 reflections from which 865 were independent with $I \geq 2\sigma(I)$, the final values are $R=0.042$, $R_\omega=0.045$, and $S_\omega=0.99$ ($R_{\text{int}}=0.022$). In this case the experimental data are not so good as for the previous structures on account of the presence of three beryllium windows in front of the sample in the helium cryostat.

The positional atomic parameters and their estimated deviations in the DNP monomer crystal at $T=296$ K, $T=145$ K, and $T=5$ K are given, respectively, in Tables I, II, and III. The atom designations in the noncentrosymmetric molecule at $T=5$ K refer to Fig. 1; at $T=296$ K and $T=145$ K labeling is the same for each half molecule. The isotropic thermal coefficients of the starred hydrogen atoms were fixed at 4 Å^2 (atomic parameters at $T=296$ K and $T=145$ K) and at 2 Å^2 (atomic parameters at $T=5$ K). Anisotropically refined atoms are given in the form of the isotropic equivalent displacement parameters defined as

$$B_{\text{eq}}=\tfrac{4}{3}\cdot(a^2\cdot B_{11}+b^2\cdot B_{22}+c^2\cdot B_{33}+ab\cos\gamma\cdot B_{12}+ac\cos\beta\cdot B_{13}+bc\cos\alpha\cdot B_{23})\,.$$

Lattice parameters of DNP monomer crystal are given in Table IV for four temperatures: $T=293$ K, $T=145$ K, $T=70$ K, and $T=5$ K. It results a continuous contraction of a,b,c dimensions versus temperature, an increas-

TABLE III. Positional parameters for DNP atoms and equivalent isotropic displacement parameters at $T=5$ K, with estimated standard deviation in parentheses.

Atom	X	Y	Z	B(Å^2)
*O*1	0.281(1)	0.357	0.0726(3)	0.6(1)
*O*2	0.229(1)	0.3309(4)	−0.1027(3)	1.1(1)
*O*3	0.585(1)	0.2766(4)	−0.1551(3)	0.9(1)
*O*4	1.184(1)	0.0154(4)	0.0122(3)	0.7(1)
*O*5	1.219(1)	0.0056(4)	0.1599(3)	0.9(1)
*O*11	1.173(1)	0.7956(3)	0.4183(2)	0.72(9)
*O*12	1.308(1)	0.8172(4)	0.5936(3)	0.89(9)
*O*13	0.987(1)	0.8692(4)	0.6663(2)	0.9(1)
*O*14	0.333(1)	1.1346(4)	0.5330(3)	1.1(1)
*O*15	0.225(1)	1.1446(4)	0.3845(3)	1.0(1)
*N*1	0.451(1)	0.2887(4)	−0.0933(3)	0.6(1)
*N*2	1.117(1)	0.0417(4)	0.0846(3)	0.5(1)
*N*11	1.087(1)	0.8600(4)	0.5964(3)	0.8(1)
*N*12	0.368(1)	1.1074(4)	0.4541(3)	0.6(1)
*C*1	0.617(2)	0.5414(6)	0.2284(4)	1.3(2)
*C*2	0.432(2)	0.4791(5)	0.1995(4)	0.4(1)
*C*3	0.219(2)	0.4037(5)	0.1567(4)	0.9(1)
*C*4	0.483(1)	0.2812(5)	0.0795(4)	0.3(1)
*C*5	0.619(2)	0.2365(5)	0.1630(4)	0.6(1)
*C*6	0.819(2)	0.1575(5)	0.1630(4)	0.7(1)
*C*7	0.892(2)	0.1234(5)	0.0836(4)	0.5(1)
*C*8	0.774(1)	0.1668(5)	−0.0018(4)	0.3(1)
*C*9	0.570(1)	0.2451(5)	−0.0016(4)	0.3(1)
*C*11	0.826(2)	0.6128(5)	0.2631(4)	0.5(1)
*C*12	1.002(2)	0.6782(5)	0.2903(4)	0.8(1)
*C*13	1.210(2)	0.7566(5)	0.3273(4)	0.7(1)
*C*14	0.976(2)	0.8708(5)	0.4243(4)	0.4(1)
*C*15	0.808(2)	0.9172(5)	0.3473(4)	1.0(1)
*C*16	0.620(1)	0.9950(5)	0.3561(4)	0.4(1)
*C*17	0.579(2)	1.0279(5)	0.4450(4)	1.0(1)
*C*18	0.736(2)	0.9822(5)	0.5216(4)	0.6(1)
*C*19	0.930(2)	0.9043(5)	0.5102(4)	1.2(2)
*H*3*A*	0.16(3)	0.349(9)	0.193(6)	2.0*
*H*3*B*	0.06(3)	0.461(8)	0.133(6)	2.0*
*H*5	0.57(2)	0.261(8)	0.204(6)	2.0*
*H*6	0.90(2)	0.131(8)	0.211(6)	2.0*
*H*8	0.82(2)	0.150(9)	−0.052(6)	2.0*
*H*13*A*	1.21(2)	0.820(8)	0.296(6)	2.0*
*H*13*B*	1.40(3)	0.704(8)	0.351(6)	2.0*
*H*15	0.80(2)	0.897(8)	0.278(6)	2.0*
*H*16	0.52(2)	1.020(8)	0.307(6)	2.0*
*H*18	0.66(2)	0.993(8)	0.568(6)	2.0*

TABLE IV. Lattice parameters of DNP monomer crystal versus temperature.

T/K	a/Å	b/Å	c/Å	β/deg	V/Å^3
296	5.189(5)	11.932(5)	14.729(5)	98.56(4)	901.7
145	5.126(5)	11.829(5)	14.698(5)	98.81(4)	880.7
70	5.082(10)	11.79(2)	14.66(2)	98.8(1)	866.5
5	5.036(10)	11.76(1)	14.66(2)	98.9(1)	857

ing in β value and a 5.3% decrease in unit cell volume between room temperature and $T=5$ K.

B. Molecular configuration

As we have already shown, there is a loss of molecular centrosymmetry in the low-temperature structure of DNP monomer crystal, deduced from the loss of systematic extinctions for the $h0l$ reflections with $h+l=2n$: it leads to space group $P2_1(Z=2)$ and appears on Fig. 2, which is a stereodrawing of the unit cell with two molecules at $T=5$ K.

In the high-temperature phase, the planes of the two benzene rings are parallel and the molecule is centrosymmetric. At $T=5$ K, in the low-temperature phase, the main structural change corresponds to 5.1° intramolecular twisting between the planes of the two aromatic groups: Figure 3 shows this small rearrangement in DNP molecules when they are projected on the plane (ab) along the c axis. There is no appreciable reorientation of NO_2 substituents with respect to benzene rings: at $T=5$ K the values of the angles between the two planes (for the two inequivalent DNP moieties) are, respectively, 2.9° and 1.6° for one of the NO_2 substituents and 20.4° and 20.7° for the other, whereas these values decrease, respectively, from 4.7 to 1.7 and 24.4 to 20.2 from 296 to 145 K.

Other interesting results are the values of the torsion angles at the joint of the diacetylene rod and the benzene rings, which are compiled in Table V. At $T=5$ K, the two given values are for the two moieties of the DNP molecule; the values in parentheses correspond to the higher numbers of the labeled atoms (Fig. 1).

IV. PROTON NMR IN DNP MONOMER CRYSTALS

A. Proton spectrum at room temperatures

A typical proton NMR spectrum of DNP is shown in Fig. 4. The spectrum of DNP can be understood by considering only magnetic dipolar coupling of protons at different sites. The spectrum consists of a broad central line at the proton Larmor frequency and up to four resolved, symmetrically split satellite lines. The broadening of these lines and also the separation of the satellite lines vary according to the orientation of the magnetic field with respect to the proton-proton distance vectors. Using the results of the x-ray study we were able to simulate the spectra and to assign the lines to the different proton positions.

Due to the $P2_1/n$ symmetry, there are two magnetically inequivalent orientations of the proton-proton distance vector of the protons $H3A$ and $H3B$ which explain the four satellite lines caused by the short distances ($r=1.56$ Å) of the protons $H3A$ and $H3B$ if the magnetic field is rotated in a plane perpendicular to crystal a axis. The well-resolved doublet splitting $\delta\nu$ is given by

$$\delta\nu=\frac{3}{2}\frac{\gamma_P^2\hbar^2}{r_{12}^3}(1-3\cos^2\theta)\ . \tag{4.1}$$

θ is the angle between the $H3A$-$H3B$ axis and the direction of the magnetic field, $\hbar$ is Planck's constant, and γ_P

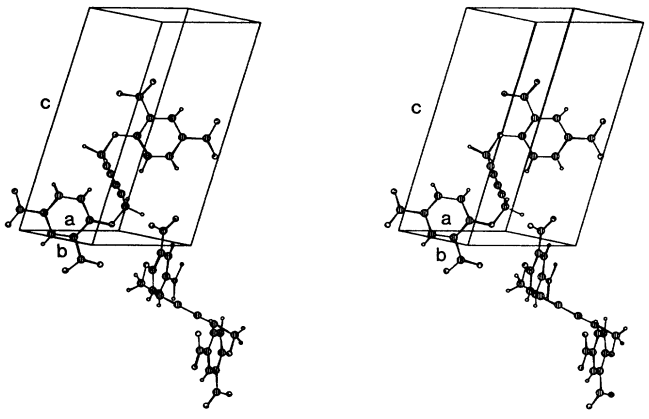

FIG. 2. Stereodrawing of the molecular arrangement at $T=5$ K in a DNP monomer crystal for one unit cell and two molecules ($Z=2$).

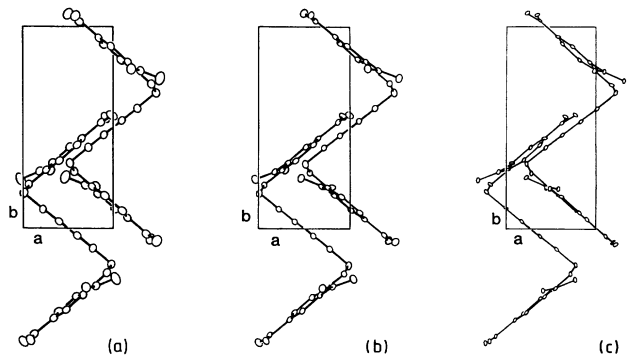

FIG. 3. Packing arrangement of DNP molecules in the monomer crystal as viewed along the c axis (thermal ellipsoids 50% probability) at three temperatures: (a) $T=296$ K, (b) $T=145$ K, (c) $T=5$ K.

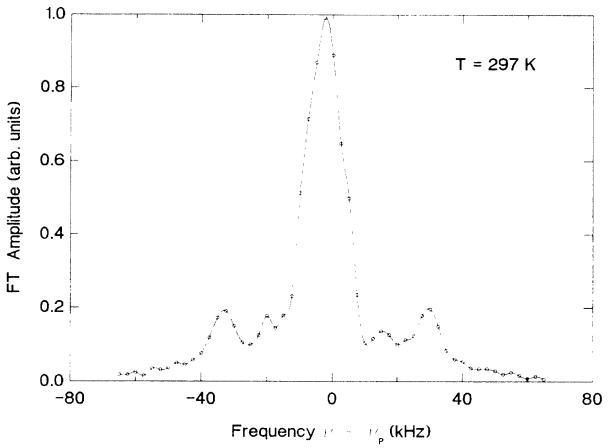

FIG. 4. ^{1}H spectrum of a DNP single crystal recorded at room temperature (ν_P=200 MHz) for a axis of the crystal oriented perpendicular to the external field.

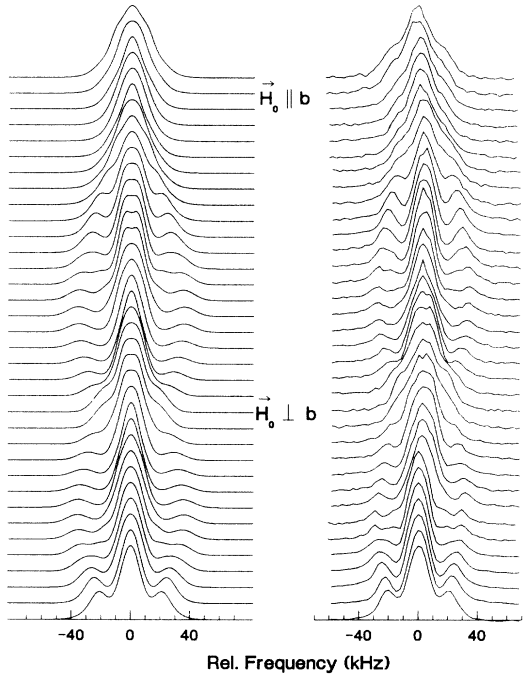

FIG. 5. Simulated (left) and experimental (right) proton spectra as a function of the orientation of the crystal with respect to the external magnetic field recorded at room temperature (ν_P=200 MHz). The crystal was rotated by steps of 5° around its long axis (a axis), which was oriented perpendicular to the external field. The simulation of the spectra is explained in detail in the text.

is the gyromagnetic ratio of the proton. The central line is preponderantly due to the protons $H5, H6, H8$. The lines are broadened by contributions to the second moment from all of the neighbor protons.

Rotating the crystal around its a axis, which was oriented perpendicular to the external magnetic field, results in an angle-dependent spectra pattern shown in Fig. 5. A rotation pattern with simulated spectra is given for comparison with these experimental data. The simulation is done by using a detailed second-moment calculation and adopting the coordinates of the protons from the x-ray analysis.

Each simulated spectrum is built up by 2×8 lines with an assumed Gaussian shape and appropriate width. 2×2 stem from the aliphatic protons $H3A$ and $H3B$ ($H13A$ and $H13B$) and 2×6 from the aromatic protons. The positions of these lines are calculated with the help of Eq. (4.1). Their intensities are assumed to have a ratio of 1:2, reflected by the ratio of the areas of the satellite line to the middle line, based on the assumption that the nuclear spins of the protons $H3A$ and $H3B$ build up a triplet, whereas the nuclear spins of $H5$, $H6$, and $H8$ behave independently. The half-width of the individual Gaussian line is given by the second moment[11]

$$\langle \Delta\omega^2 \rangle = \tfrac{3}{4}\gamma_P^4 \hbar^2 I(I+1) \sum_k \frac{(1-3\cos^2\theta_{jk})^2}{r_{jk}^6} . \qquad (4.2)$$

This simulation describes the orientation dependence of the experimental data satisfactorily. Evidently for favorable orientations of the single crystal the separation and the shape of the satellite lines indicate changes in the molecular orientation with a resolution of better than 5°.

TABLE V. Values of the torsion angles in degrees at 296, 145, and 5 K.

	296 K	145 K	5K
C5-C4-O1-C3	−4.8	−4.2	−2.4(6.2)
C9-C4-O1-C3	174.5	175.1	176.9(−172.1)
C4-O1-C3-C2	−72.5	−72.9	−74.0(69.6)

B. Temperature dependence of the proton spectrum

Making use of this sensitivity we are able to discern the rather small temperature dependent changes of the proton NMR spectrum (Fig. 6). There is a small visible shift and splitting (or at least broadening) of the satellite lines (besides a non-negligible broadening of the central line) for temperatures decreasing below the ferroelectric phase transition at T_c=46 K. There are no discontinuities at the ferroelectric phase transition, however.

A small reorientation of the DNP molecules relative to the unit cell and the macroscopic outer dimensions of the crystal during the phase transition could explain these changes. A more clear-cut interpretation of the NMR-spectral changes can be obtained by comparison with the x-ray results. Besides a reorientation of the DNP molecules with respect to the crystal axis c [or c^*, perpendicular to the (ab) plane] by about 3°, which might be fictitious due to the change of the space group from $P2_1/n$ to $P2_1$, the x-ray analysis reveals clearly an intramolecular twisting of the central diacetylene unit, where the two parts of each DNP molecule turn around the single bond $C1$—$C11$ in opposite directions. This is illustrated in Fig. 7. These reorientations of the CH_2 groups explain

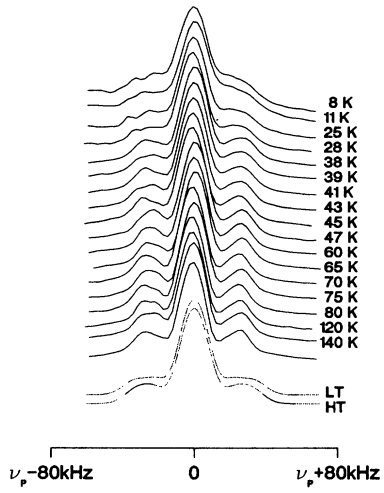

FIG. 6. Variation of the proton spectra of a DNP single crystal with temperature for fixed orientation of the single crystalline sample with the a axis perpendicular to the external field ($\nu_P = 200$ MHz). The changes of the satellite line shapes for $T < 47$ K can clearly be seen. Below that two simulated spectra are shown as a guide to the eye for the two different crystallographic phases (LT: low-temperature, HT: high-temperature phase).

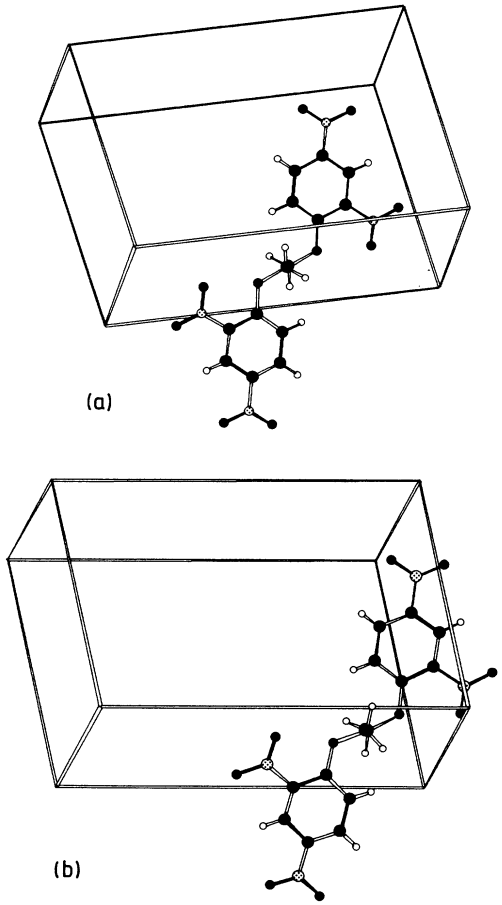

FIG. 7. Projection of a DNP molecule along the $C3$-$C13$ axis. (a) $T = 145$ K, (b) $T = 5$ K. This projection reveals the reorientation of the CH_2 groups in the ferroelectric phase (compare $H3A$-$H3B$ and $H13A$-$H13B$).

the changes observed for the satellite lines in the proton-NMR spectra (Fig. 6).

C. Proton spin-lattice relaxation

The temperature dependence of the spin-lattice relaxation rate is shown is Fig. 8. It was measured at three different frequencies (31, 60, and 200 MHz) in a temperature range between 20 and 300 K. The observed temperature dependence allows to assume two rate maxima. Both maxima show qualitatively the same behavior when the temperature is lowered: With lower frequency the maxima are shifted to lower temperatures and become more pronounced in height but smaller in width: a typical appearance of a relaxational mechanism described by the model of Bloembergen, Purcell, and Pound.[12] The spin-lattice relaxation rate $1/T_1$ caused by dipole dipole interaction between proton nuclear spins is given by[11]

$$\frac{1}{T_1} = \frac{3}{2}\gamma_P^4 \hbar^2 I(I+1) \sum \{J_{ik}^1(\omega_I) + J_{ik}^2(2\omega_I)\} , \quad (4.3)$$

where $\hbar$ is Planck's constant, γ_P is the gyromagnetic ratio, I the nuclear spin of the proton ($I = \frac{1}{2}$), and J_{ik} is the spectral intensity of the relaxational process. The spectral intensities are obtained from the Fourier spectra of the position coordinates

$$F^1 = \sin\theta_{ik} \cos\theta_{ik} e^{i\phi_{ik}} \frac{1}{r_{ik}^3} ,$$
$$F^2 = \sin^2\theta_{ik} e^{2i\phi_{ik}} \frac{1}{r_{ik}^3} , \quad (4.4)$$

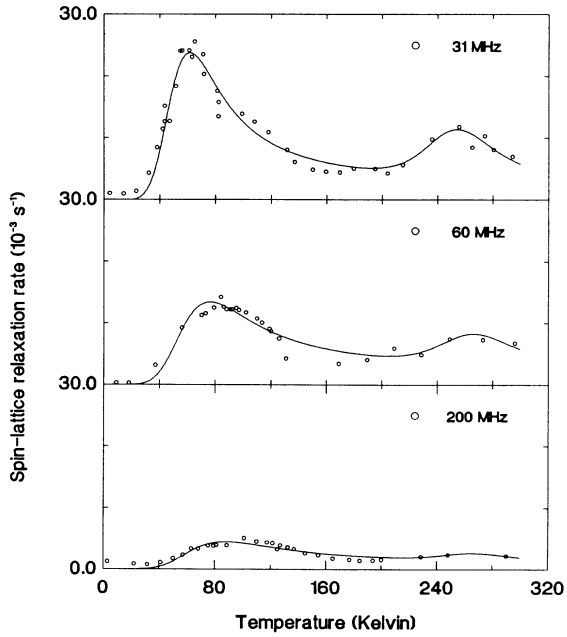

FIG. 8. Spin-lattice relaxation rate of the protons in a DNP monomer single crystal for three Larmor frequencies. Two rate maxima can be discerned with a temperature dependence explained by the model of Bloembergen, Purcell, and Pound. The solid line shows the fit with this model assuming two rate maxima (see text).

with $J(\omega)=\langle F(t)F^*(t)\rangle_{av}2\tau_c(1+\omega^2\tau_c^2)^{-1}$ and τ_c is a correlation time. In a simple approach, τ_c may be assumed to be of the form

$$\tau_c=\tau_0 e^{E/k_BT}, \tag{4.5}$$

where E is an activation energy corresponding approximately to the height of the potential barrier between two characteristic molecular positions and k_B is Boltzmann's constant. Since the individual contribution to the relaxation depends strongly on the distance, it is obvious to assume that the methylene group protons ($H3A$, $H3B$ and $H13A$, $H13B$) might predominate in the relaxational contribution, especially after the reorientation of these groups at the ferroelectric phase transition is established. Under such conditions, the strong orientation dependence of this contribution in Eq. (4.4) should be observable. Thus, we checked whether there is also an angle dependence of the measured spin-lattice relaxation time. These measurements were carried out, respectively, at 130 and at 300 K. However, in Fig. 9 it is not possible to discern any angle dependence outside the error bars for the low-temperature maximum.

Furthermore we compared the spin-lattice relaxation rate for applying the external field parallel or perpendicular to the a axis of the crystal. Also for these orientations we got only slightly (10%) different values for T_1. At 130 K the $\sin^2\theta$ term preponderates for the relaxation process[11] and so there would be an angle dependence of the relaxation rates if only the modulation of one characteristic proton-proton separation or orientation predominated in Eq. (4.3).

We have also checked up on a possible orientation dependence of the high-temperature maximum, but the relaxation data at $T=300$ K recorded at 60 MHz revealed no orientation dependence, too. The absence of any clear orientation dependence of the spin-lattice relaxation for the low- and high-temperature maxima indicates that there are many proton-proton distances and orientations which are modulated by the molecular vibrational or librational motion. In this situation Eq. (4.3) can be approximated by

$$\frac{1}{T_1}=\delta(\Delta\omega^2)_{LT}\left[\frac{\tau_{c,LT}}{1+\omega^2\tau_{c,LT}^2}+\frac{4\tau_{c,LT}}{1+4\omega^2\tau_{c,LT}^2}\right]+\delta(\Delta\omega^2)_{HT}\left[\frac{\tau_{c,HT}}{1+\omega^2\tau_{c,HT}^2}+\frac{4\tau_{c,HT}}{1+4\omega^2\tau_{c,HT}^2}\right]. \tag{4.6}$$

Here $\delta(\Delta\omega^2)_{HT}$ and $\delta(\Delta\omega^2)_{LT}$ are the average variance of the relevant second moments. They are determined experimentally. The value of $\delta(\Delta\omega^2)$ affords an intuitive understanding of the strength of the relaxational process.

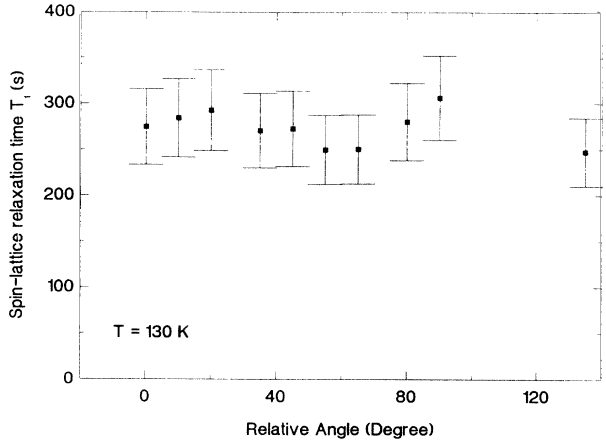

FIG. 9. Dependence of the spin-lattice relaxation rate of the protons on the angle with respect to the external magnetic field ($\nu_P=200$ MHz). The monomer single crystal was turned around its a axis. The angular variation of the relaxation rate resided in the error limit.

The results of the fit are summarized in Table VI. The activation energies of 20 meV and 0.3 eV, derived here for the low- and high-temperature relaxation process, respectively, can be compared with the energies that have been observed for librational and vibrational molecular motions in other diacetylenes, before.[13] Librational modes of very low energy were considered before[14,15] in connection with a structural phase transition in the diacetylene bis(p-toluene sulphonate) of 2,4-hexadiyne-2,6 diol (pTS). pTS is the most thoroughly investigated diacetylene, where the side group is $CH_2-O-SO_2-C_6H_4-CH_3$. At about 185 K pTS shows a doubling of the unit cell in a low-temperature phase of both polymer and monomer. The second-order nature of the phase transition has been deduced from far-IR studies,[14] where modes have been found with characteristic soft-mode behavior. Thus, we also assume that the low-temperature rate maximum is caused by a librational mode inducing the phase transition of DNP.

We have to point to the fact, however, that we have detected this supposed librational twisting mode in the high-temperature phase and that we were able to describe its relaxational contribution with a constant activation energy for temperatures above 60 K, where the proton relaxation rate for Larmor frequencies of 31 MHz and above is sensitive to the motional time scale in question. A critical behavior like a mode softening is not observed in the temperature and frequency range of our NMR investigation. This is not unfamiliar for ferroelectric transi-

TABLE VI. Results of the fit according to the BPP model using two rate maxima [Eq. (4.6)].

	LT maximum	HT maximum
Average variance in second moment $\delta(\Delta\omega^2)$	11.0×10^6 s^{-2}	4.0×10^6 s^{-2}
Activation energy E	1.9 kJ/mole	27 kJ/mole
Prefactor τ_0	72 ps	8 fs

tions,[16] however.

Also for the explanation of the activation energy connected with the high-temperature relaxation maximum the comparison with pTS provides a possible answer. The Raman spectra of this compound exhibit four prominent bands, one of them at 2086 cm^{-1} (0.26 eV). More specifically, Niederwald[17] found values of 0.2–0.4 eV for the activation energies required for the rate equations describing the stepwise SSP in the uv-polymerization studies of the diacetylene pTS. Since we found a similar value for the activation energy from our NMR studies (Table VI), we assume that it reflects the type of molecular motion that is characteristic for the thermal SSP of DNP. A detailed optical investigation of DNP would be interesting to clarify the assignment of both types of motions.

For an additional characterization of the origin of these two rate maxima we investigated a polymerized DNP crystal, too.

D. Influence of solid-state polymerization

We used for the NMR analysis a crystal which had a polymer content of about 95%. The polymerization of diacetylenes is a well-investigated topochemical reaction (for an overview see, e.g., Ref. 18). As we have earlier remarked, the DNP crystals will be polymerized up to 95% after 16 h at 130 °C, which was proved gravimetrically. A longer polymerization time causes an order-disorder transition. The latter was also confirmed by static magnetic susceptibility measurements, which showed an increased content of paramagnetic defects by up to 2 orders of magnitude for longer polymerization times than 16 h, whereas the number of paramagnetic defects counted with this method was approximately equal for monomer and polymer crystals of up to 95% polymer content. It was generally lower than 1 spin ($S=\frac{1}{2}$) per 10 000 DNP molecules.

For the monomer crystals, we could exclude a significant contribution to the spin-lattice relaxation by spin-diffusion to paramagnetic defects based on the temperature and frequency dependencies of the single exponential relaxation observed. Due to the equally low content of paramagnetic centers in the partially polymerized crystals, we assumed the insignificance of their relaxational contribution here, too. Only crystals polymerized much longer than 16 h showed a significantly shorter spin-lattice relaxation time due to their increased content of paramagnetic defects.

Since the high-temperature maximum of the proton spin-lattice relaxation rate of the monomer crystal was already not very pronounced we were not able to decide on its existence in the polymerized crystal on the basis of the measured temperature dependence of the spin-lattice relaxation rate. We could clearly exclude the existence of the low-temperature maximum for the polymerized crystal, however. This gives further evidence for our conclusion that the low-temperature spin-lattice relaxation rate maximum is induced by the librational mode which is responsible for the phase transition and which must therefore be absent in a polymerized crystal, since the polymerization suppresses the phase transition.

V. CONCLUSIONS

The x-ray structural analysis reported above proves that monomer crystals of the diacetylene DNP [1,6-bis(2,4-dinitrophenoxy)-2,4-hexadiyne] have a homogeneous ferroelectric low-temperature phase with a weak, but uniform molecular distortion in every unit cell. The most prominent structural change is the intramolecular twisting of the two aromatic groups by about 5.1°. Since these rings carry the NO_2 groups mainly responsible for the electric dipole moments, this deviation from centrosymmetry explains the observed ferroelectric behavior.

The proton NMR spectrum reflects the orientation of the proton-proton axis of the methylene groups close to the central diacetylene unit in a rather clear-cut way. The spectral changes resulting from the rotation of a single crystal in the external magnetic field could be explained. More important, the variation of the spectrum for temperatures lower than the temperature of the ferroelectrical phase transition for unchanged orientation of the single crystal proved a molecular reorientation, that was identified by combining NMR and x-ray data as an intramolecular twisting around the central single bond of the diacetylene unit.

This is an experimental result of particular importance, because it explains, why the ferroelectric phase transition of DNP is suppressed by the solid-state polymerization: evidently this torsion of the central diacetylene part is necessary for and correlated with the phenyl ring rotation. Since the central diacetylene unit is fixed in the polymer backbone for the polymerized DNP crystal, also the ferroelectric phase transition is suppressed.

One of the most interesting questions tackled with the present investigation was the inquiry whether molecular motions could be identified in the high-temperature phase of DNP that induce the phase transition to the noncentrosymmetric low-temperature phase. We have shown, that proton spin-lattice relaxation reflects two different modes of molecular motions. One type with a characteristic activation energy of about 0.3 eV is not special for DNP and seems to be related with vibrational and librational degrees of freedom that are also engaged in the solid-state polymerization process. It influences mainly the high-temperature proton relaxational behavior. A second mode with a very low activation energy of about 20 meV was tied to a librational twisting mode as it is known from other diacetylenes. This mode might induce the static reorientations responsible for the low-temperature ferroelectric properties of DNP and reflected by the x-ray data and NMR study reported above. It will be interesting to substantiate these arguments by a detailed optical investigation of these low-energy modes of DNP.

ACKNOWLEDGMENTS

We thank I. Müller for growing the single crystals. We are indebted to P. Gruner-Bauer, U. Haeberlen, M. Schwoerer, and P. Strohriegl for discussions. This work was supported by the Emil Warburg Stiftung and by the Deutsche Forschungsgemeinschaft (Sonderforschungsbereich 213, TOPOMAK, Bayreuth). Groupe de Physique Cristalline is Unité de Recherche Associée au CNRS No. 040804.

---

*Present address: Physikalisches Institut, Universität Karlsruhe (TH), Postfach 6980, W-7500 Karlsruhe, Germany.

[1]H. Schultes, P. Strohriegl, and E. Dormann, Ferroelectrics **70**, 161 (1986).

[2]G. F. Lipscomb, A. F. Garito, and T. S. Wei, Ferroelectrics **23**, 161 (1980).

[3]A. R. McGhie, G. F. Lipscomb, A. F. Garito, K. N. Desai, and P. S. Kalyanaraman, Makromol. Chem. **182**, 965 (1981).

[4]M. Bertault and L. Toupet, Mater. Sci. **13**, 23 (1987).

[5]P. Gruner-Bauer and E. Dormann, J. Phys. Condens. Matter **4**, 5599 (1992).

[6]P. A. Albouy, Thesis, Paris, 1982.

[7]P. S. Kalyanaraman, A. F. Garito, K. N. McGhie, and K. N. Desai, Makromol. Chem. **180**, 1393 (1979).

[8]B. A. Frenz, ENRAF-NONIUS structure determination package, SDP users guide, College Station, Texas 77840 and Enraf-Nonius, Delft, Netherlands, 1985.

[9]*International Tables for X-Ray Crystallography* (Kynoch Birmingham, 1974), Vol. 4 (present distributor D. Reidel, Dordrecht).

[10]P. Main, S. J. Fiske, S. E. Hull, L. Lessinger, G. Germain, I. P. Declercq, and M. M. Woolfson, MULTAN 82 (a system of computer programs for the automatic solution of crystal structures from x-ray diffraction data), University of York, England and Louvain, Belgique, 1982.

[11]A. Abragam, *The Principles of Nuclear Magnetism* (Oxford University Press, Oxford, England, 1961).

[12]N. Bloembergen, E. M. Purcell, and R. V. Pound, Phys. Rev. **73**, 679 (1948).

[13]D. N. Batchelder and D. Bloor, in *Advances in Infrared and Raman Spectroscopy,* edited by R. J. H. Clark and R. E. Hester (Wiley, New York, 1984), Vol. 11.

[14]D. Bloor and R. J. Kennedy, Chem. Phys. **47**, 1 (1980).

[15]J. P. Aime, M. Schott, M. Bertault, and L. Toupet (unpublished).

[16]S. Elschner and J. Peterson, Z. Phys. B **52**, 37 (1983); H. D. Maier and J. Peterson, Solid State Commun. **45**, 175 (1983).

[17]M. Schwoerer and H. Niederwald, Makromol. Chem. Suppl. **12**, 61 (1985).

[18]H. Sixl, in *Advances in Polymer Science,* edited by H.-J. Cantow (Springer-Verlag, New York, 1984), Vol. 63.